$^{87}Sr/^{86}Sr$ stratigraphy from the Early Triassic of Zal, Iran: Linking temperature to weathering rates and the tempo of ecosystem recovery

Alexa R.C. Sedlacek[1,2], Matthew R. Saltzman[2], Thomas J. Algeo[3], Micha Horacek[4,5], Rainer Brandner[6], Kenneth Foland[2], and Rhawn F. Denniston[7]

[1]Department of Earth Science, University of Northern Iowa, 121 Latham Hall, Cedar Falls, Iowa 50614, USA
[2]School of Earth Sciences, Ohio State University, Columbus, Ohio 43210, USA
[3]Department of Geology, University of Cincinnati, Cincinnati, Ohio 45221, USA
[4]BLT Wieselburg, Research Center Francisco-Josephinum, Rottenhauser Strasse 1, 3250 Wieselburg, Austria
[5]Department of Lithospheric Research, Althanstrasse 14, Vienna University, 1090 Vienna, Austria
[6]Institute of Geology and Paleontology, University of Innsbruck, Innrain 52, 6020 Innsbruck, Austria
[7]Department of Geology, Cornell College, Mount Vernon, Iowa 52314, USA

ABSTRACT

Recovery from the Late Permian mass extinction was slowed by continued environmental perturbations during the Early Triassic. Rapid fluctuations of the Early Triassic marine carbonate carbon isotope record indicate instability in the global carbon cycle, and recent $\delta^{18}O_{apatite}$ studies link elevated temperatures to the prolonged biotic recovery. High temperatures potentially caused enhanced continental weathering that was detrimental to marine ecosystems, but linking weathering rates to temperature has proven difficult. One proxy for weathering is the $^{87}Sr/^{86}Sr$ of marine carbonate; we present here an $^{87}Sr/^{86}Sr$ record from an upper Permian–lower Triassic succession near Zal, Iran, that is coupled to a $\delta^{13}C_{carbonate}$ record. An increase in the rate of $^{87}Sr/^{86}Sr$ rise from the Dienerian to the Smithian may be linked to elevated continental weathering rates caused by warming during the Smithian.

INTRODUCTION

The Early Triassic was a period of protracted recovery from the Late Permian mass extinction, which devastated marine and terrestrial ecosystems (e.g., Retallack, 1995; Erwin et al., 2002; Payne et al., 2006; Algeo et al., 2011). The Early Triassic was also characterized by instability in the carbon cycle and global temperature fluctuations, suggesting that biotic recovery may have been inhibited by persistent environmental disturbances (Payne et al., 2004; Sun et al., 2012). Payne and Kump (2007) proposed that the oscillatory nature of the Early Triassic marine carbonate $\delta^{13}C$ record (e.g., Payne et al., 2004; Horacek et al., 2007) was linked to warming caused by episodic pulses of volcanism from the Siberian Traps and related changes in weathering rates and organic carbon burial. Increased sedimentation rates (Algeo and Twitchett, 2010) and extreme temperature changes (Sun et al., 2012) may have contributed to the prolonged interval of recovery of marine ecosystems following the end-Permian biological crisis.

The details of the timing of the Early Triassic recovery are emerging as higher-resolution biodiversity curves are constructed using improvements in the geologic time scale. Low diversity levels characterize the Early Triassic Griesbachian (early Induan) substage, and the recovery of several clades coincided with cooling during the Dienerian (late Induan) substage (Payne et al., 2006; Stanley, 2009; Song et al., 2011; Sun et al., 2012). A subsequent loss of diversity during the late Smithian (early Olenekian) substage may have been a result of the elevated temperatures of the late Smithian thermal maximum (Sun et al., 2012). The $\delta^{18}O_{apatite}$-based paleotemperature curve from the Early Triassic of Sun et al. (2012) makes important predictions about increased continental weathering rates that may have contributed to delayed recovery of marine ecosystems. We have sought to test this link between temperature, weathering, and delayed faunal recovery based on marine carbonate $^{87}Sr/^{86}Sr$. Enhanced continental weathering is thought to be the main contributor to the large and rapid global increase of seawater $^{87}Sr/^{86}Sr$ (~0.7070–0.7082) during the latest Permian–Early Triassic (Martin and Macdougall, 1995; Korte et al., 2003, 2004, 2006; Huang et al., 2008), but changes in the rate of $^{87}Sr/^{86}Sr$ increase have yet to be examined due to limitations on both sampling density and radiometric age control.

Here we present an $^{87}Sr/^{86}Sr$ time series generated from bulk carbonate samples from a Late Permian–Early Triassic section at Zal, Iran (Fig. 1), that was located in the central Tethys Ocean (Fig. DR1 in the GSA Data Repository[1]). This section is biostratigraphically well constrained and was previously analyzed for carbonate carbon isotopes (Horacek et al., 2007; for paleogeographic and biostratigraphic details, see the Data Repository). Our study is the first high-resolution analysis of strontium isotopic variation through the Early Triassic that is coupled with a $\delta^{13}C_{carbonate}$ record from the same field site. We relate these isotope data to paleotemperatures through comparison with the $\delta^{18}O_{apatite}$ record of Sun et al. (2012).

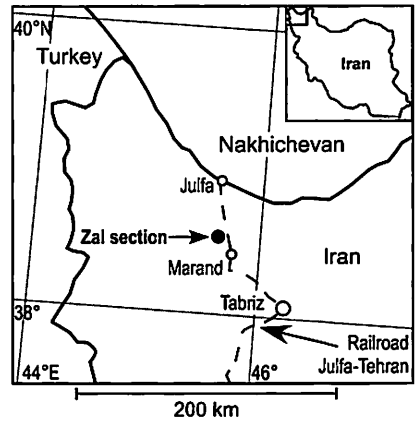

Figure 1. Location of Zal, Iran, section (38°43′47″N, 45°36′13″E, 1600 m), modified from Horacek et al. (2007).

BACKGROUND

Spatial homogeneity of seawater $^{87}Sr/^{86}Sr$ ratios is maintained because the residence time of Sr in the ocean is ~10^6 yr, which vastly exceeds the oceanic mixing time of ~10^3 yr (Veizer, 1989). Marine carbonates show systematic changes in seawater $^{87}Sr/^{86}Sr$ at geologic time scales, providing a chemostratigraphic tool (Veizer et al., 1999; Martin and Macdougall,

[1]GSA Data Repository item 2014283, paleogeography and biostratigraphy of the Zal section, Early Triassic time scale and sedimentation rates, seawater Sr isotope model description and results, Table DR1 ($^{87}Sr/^{86}Sr$ results and age assignments), Table DR2 (Late Permian–Middle Triassic time scale), and Table DR3 (model results), is available online at www.geosociety.org/pubs/ft2014.htm, or on request from editing@geosociety.org or Documents Secretary, GSA, P.O. Box 9140, Boulder, CO 80301, USA.

1995; Korte et al., 2003, 2004, 2006; Huang et al., 2008). Seawater $^{87}Sr/^{86}Sr$ is predominantly controlled by inputs of Sr at mid-ocean ridges through hydrothermal exchange, and from rivers that carry Sr ions weathered from continental source rocks to the oceans (Palmer and Edmond, 1989). The hydrothermal flux is enriched in ^{86}Sr, and has a nearly uniform $^{87}Sr/^{86}Sr$ of ~0.703 (Albarède et al., 1981). However, the riverine flux is enriched in ^{87}Sr (modern global average riverine $^{87}Sr/^{86}Sr$ is ~0.712), which is derived from the decay of ^{87}Rb in crystalline terrains, and its concentration and isotopic value are highly variable due to heterogeneities in the isotopic composition of continental crust, the concentration of Sr in source rocks, and weathering rates. Thus, much of the secular variation in seawater $^{87}Sr/^{86}Sr$ is thought to result from changes in the $^{87}Sr/^{86}Sr$ and total Sr concentration of the riverine flux and changes in seafloor-spreading rates (Richter and Turekian, 1993).

The rapid increase in seawater $^{87}Sr/^{86}Sr$ during the Late Permian through Early Triassic has been well documented by analyses of brachiopod low-magnesium calcite, conodont apatite (Martin and Macdougall, 1995; Korte et al., 2003, 2004, 2006), and well-preserved micrite in bulk carbonates (Huang et al., 2008). The average rate of the Permian–Triassic rise is greater than that of the late Cenozoic (post–6 Ma) rise attributed to increased continental weathering rates linked to rapid orogenic uplift (Hodell et al., 1990; Martin and Macdougall, 1995; Korte et al., 2003).

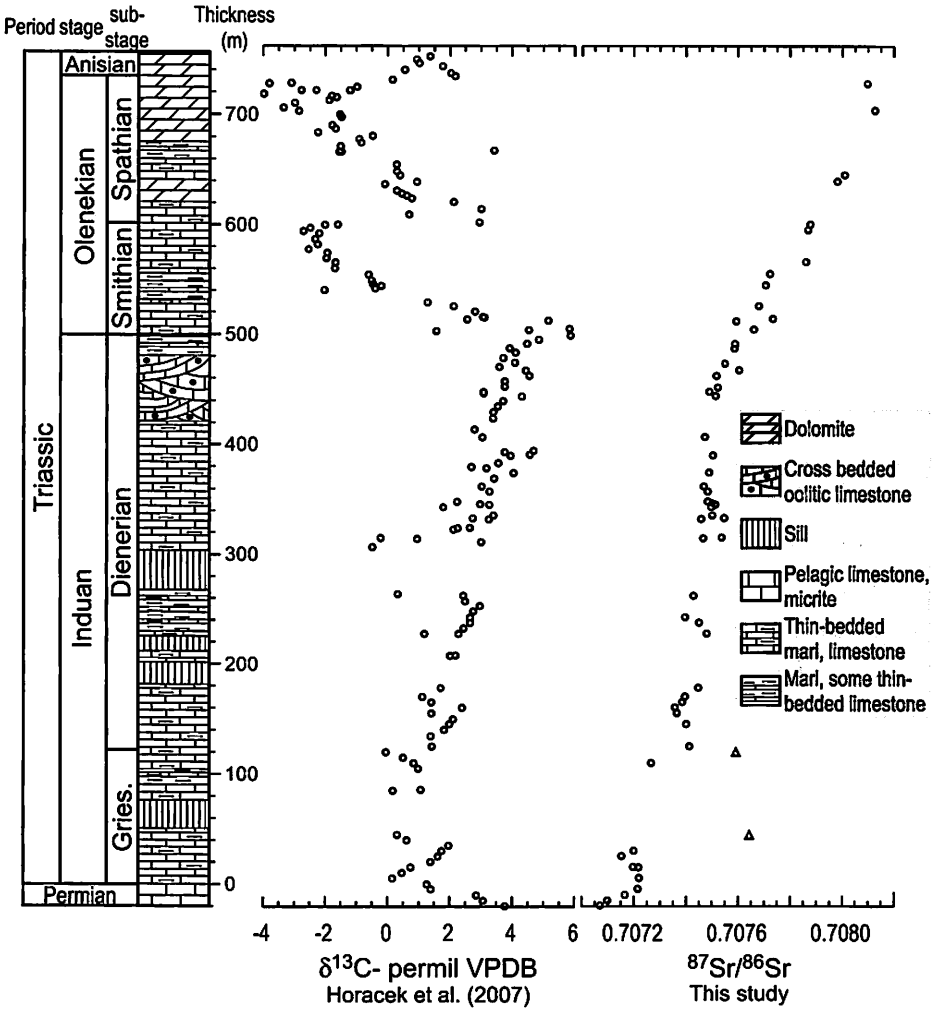

Figure 2. $\delta^{13}C$ profile for Zal, Iran (from Horacek et al., 2007) and $^{87}Sr/^{86}Sr$ data for the same sample suite. Igneous sills are present in Induan-age rocks, and their thicknesses have been subtracted from the total thickness of the Griesbachian (Gries.) and Dienerian. Samples associated with igneous sills (triangles) are considered altered and have been disregarded in further analysis. VPDB—Vienna Peedee belemnite.

METHODS AND RESULTS

We obtained 56 powdered bulk-rock samples corresponding to those analyzed for $\delta^{13}C$ by Horacek et al. (2007) and processed them for $^{87}Sr/^{86}Sr$ following the methods of Montañez et al. (1996). For each sample, ~40 mg of powder were cleaned with ultrapure 1M ammonium acetate buffered to a pH of 8, then dissolved in 4% acetic acid. The resulting supernate was spiked with an ^{84}Sr tracer, and Sr was isolated using chromatography methods calibrated to 2N HCl. Samples were loaded with HCl on a rhenium double filament configuration with a Ta_2O_5 activator, and isotopic ratios were measured using a Finnegan MAT 261A thermal ionization mass spectrometer at the Ohio State University (USA) Radiogenic Isotope Lab. The laboratory reproducibility of the standard SRM 987 is 0.710242 ± 0.000010 (1σ). Reported $^{87}Sr/^{86}Sr$ values are corrected for instrumental fractionation using normal $^{86}Sr/^{88}Sr$ of 0.119400.

Chemical analyses reveal a continuous increase in $^{87}Sr/^{86}Sr$ from the base (0.7071) to the top (0.7081) of the section (Fig. 2; Table DR1 in the Data Repository). Nearly 300 m of Dienerian-age strata account for the majority of isotope values reported, and these samples reveal a decrease in the rate of $^{87}Sr/^{86}Sr$ change [Δ(Sr)], followed by ~100 m of Smithian-age strata that show an increase in Δ(Sr) (Fig. 3). The ~130 m of Spathian rocks show a decrease in sedimentation rates during this substage relative to high sedimentation rates during the Griesbachian through Smithian (see the Data Repository for sedimentation rate calculations).

DISCUSSION

Diagenetic Alteration

Our data record the ~0.001 rise in seawater Sr isotope trends recognized for the Late Permian–Early Triassic interval in earlier studies (Korte et al., 2003, 2004, 2006; Huang et al., 2008). However, in order to determine whether Δ(Sr) varies within individual stages or zones, increased sampling density near stage boundaries is needed. Bulk-rock methods, when applied to thick stratigraphic sections such as at Zal, can provide this level of resolution, but the role of diagenesis must be addressed (Veizer et al., 1999; Waltham and Gröcke, 2006). Sr concentration is considered one of the more sensitive and reliable indicators of diagenetic alteration, which generally proceeds with loss of Sr (Veizer, 1989). At Zal, the majority of samples yielded Sr concentrations >200 ppm, and some Dienerian-age samples yielded >1000 ppm Sr (Fig. DR2). These concentrations are consistent with those reported in other studies of marine carbonates interpreted as primary seawater $^{87}Sr/^{86}Sr$ values (e.g., Montañez et al., 1996; Huang et al., 2008). Only two Griesbachian samples associated with igneous sills exhibit ^{87}Sr enrichment relative to stratigraphically adjacent samples, providing evidence of diagenetic alteration (Fig. 2). The remaining 54 samples yield $^{87}Sr/^{86}Sr$ values that define a coherent pattern of secular variation that we therefore consider to represent primary Late Permian–Early Triassic seawater values (Veizer et al., 1999). The preservation of seawater trends at Zal is also supported by comparisons with the

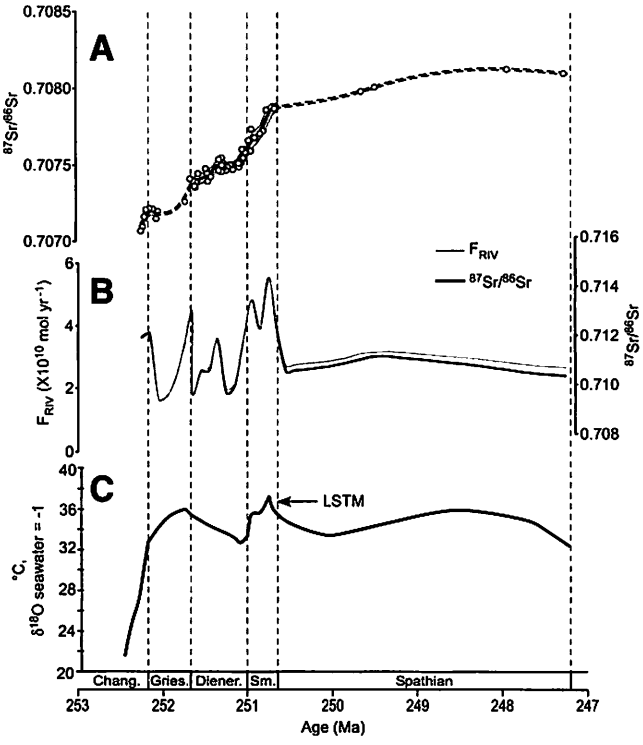

Figure 3. A: Strontium isotope profile for Zal, Iran. High-density intervals of data set were fitted with LOWESS (locally weighted scatterplot smoothing; running average) curves (black; standard deviation range is in gray); low-density intervals were fitted with spline curves (dashed line). B: Rates of change in riverine Sr fluxes (F_{RIV}, left axis; gray curves) or riverine $^{87}Sr/^{86}Sr$ ratios (right axis; black curves) needed to account for observed secular variation in $^{87}Sr/^{86}Sr$ ratios at Zal. C: Estimated sea-surface temperatures (from Sun et al., 2012). Note the late Smithian thermal maximum (LSTM). Chang.—Changhsingian; Gries.—Griesbachian; Diener.—Dienerian; Sm.—Smithian. Time scale is modified from Algeo et al. (2013) (for details, see the Data Repository [see footnote 1]).

latest Permian (Changhsingian) brachiopod data of Brand et al. (2012) that show values near ~0.7071, and the Early Triassic conodont data of Korte et al. (2004) that show values of ~0.7074–0.7077 for the *Neospathodus dieneri* conodont zone (Dienerian).

Early Triassic Time Scale

In addition to diagenesis, the Early Triassic time scale provides a source of uncertainty in the calculation of Δ(Sr) for individual stages or substages. Numeric age assignments for the boundaries of the Early Triassic substages remain a subject of debate (Gradstein et al., 2012). Δ(Sr) was calculated using the most recent radiometric and paleomagnetic age constraints, and the highest rates of change occurred during the Smithian (Wu et al., 2012; Algeo et al., 2013; for further discussion of our time scale model, see the Data Repository).

$^{87}Sr/^{86}Sr$ Model

We investigated controls on the Early Triassic rise in seawater $^{87}Sr/^{86}Sr$ using a reservoir model based on a mass balance of the three principal source fluxes of Sr to seawater: riverine, ocean-crustal hydrothermal, and marine diagenetic carbonate (Richter and Turekian, 1993). Seawater $^{87}Sr/^{86}Sr$ is influenced most strongly by (1) the Sr isotopic composition of the riverine flux (~0.712 in the modern), and (2) the ratio of the riverine and hydrothermal fluxes (1.65, based on estimated baseline fluxes of ~3.3 and 2.0×10^{10} mol yr^{-1}, respectively) (cf. Goddéris and François, 1995). For additional information concerning the model, see the Data Repository.

Observed changes in seawater $^{87}Sr/^{86}Sr$ (Fig. 3A) can be closely reproduced by the model. We investigated two scenarios to account for rising seawater $^{87}Sr/^{86}Sr$ during the Early Triassic, one in which the Sr isotopic composition of the riverine flux was held constant and the ratio of the riverine and hydrothermal fluxes was allowed to vary, and a second in which the ratio of the riverine and hydrothermal fluxes was held constant and the Sr isotopic composition of the riverine flux was allowed to vary. In the first scenario, the riverine flux of Sr rises from a low of ~2 (all values in 10^{10} mol yr^{-1}) in the Dienerian to a high of ~5 in the Smithian, before decreasing to 2 in the late Spathian (Fig. 3B). In the second scenario, the Sr isotopic composition of the riverine flux rises from ~0.711 in the Dienerian to ~0.715 in the Smithian, before returning to ~0.710 in the Spathian. Although either scenario is possible, variations in riverine Sr fluxes seem more likely in view of independent evidence of enhanced rates of subaerial erosion during the Early Triassic (Ward et al., 2000; Algeo and Twitchett, 2010).

Coupled $^{87}Sr/^{86}Sr$ and $\delta^{18}O$

In order to examine links between silicate weathering rates and temperature during the Early Triassic, we compared our data and model results to the $\delta^{18}O_{apatite}$ paleotemperature curve of Sun et al. (2012) (Fig. 3C). The Sr isotope paleoweathering and O isotope paleotemperature records show excellent first-order correspondence. The ~1.5-m.y.-long interval from the latest Permian to the end of the Smithian was associated with significant perturbations in both records, i.e., elevated weathering rates and temperatures, and the Smithian-Spathian boundary marked a transition to more stable conditions associated with reduced weathering rates and temperatures. At a finer temporal scale, the records show imperfect correspondence, possibly due to differences in sample distribution and density (and, hence, curve fidelity) but perhaps also to local influences on sea-surface temperatures between Iran and China. However, the records appear to share certain high-resolution features; e.g., rapid increases in the latest Permian and peaks in the late Griesbachian and mid-Smithian (Fig. 3). Based on these features, we infer a general causal connection between climate warming and elevated weathering rates during the Early Triassic.

The apparent link between elevated temperatures, increased weathering, and marine ecosystem stress is particularly pronounced for the Smithian substage. The middle to late Smithian was characterized by the warmest sea-surface temperatures (to >40 °C; Sun et al., 2012) as well as the highest weathering rates of the Early Triassic (Algeo et al., 2011; Fig. 3). Extreme temperatures and elevated sediment fluxes were detrimental to both benthic and pelagic marine organisms (Algeo and Twitchett, 2010), leading to elevated extinction rates among ammonoids and conodonts (Brayard et al., 2009; Stanley, 2009), size reduction of conodonts (Chen et al., 2013), and diminished speciation rates in benthic ecosystems (Song et al., 2011). In the terrestrial realm, there was a resurgence in the spread of disaster taxa (Looy et al., 1999; Saito et al., 2013).

The influence of temperature and weathering rates on ecosystem health is also evident as environmental conditions ameliorated during the Spathian substage (late Early Triassic). Sea-surface temperatures fell to <34 °C during the early Spathian (Sun et al., 2012; Fig. 3). Silicate weathering removes atmospheric CO_2 (the weathering-CO_2 feedback of Berner, 2004), and a period of rapid weathering during the latest Smithian is consistent with this cooling event (although see Goddéris et al. [2014] for an alternative view). A concurrent recovery in the diversity and abundance of some clades of marine invertebrates (Stanley, 2009; Brayard et al., 2009; Chen et al., 2013) and a return of climax conifer forests in the terrestrial realm (Looy et al., 1999; Saito et al., 2013) are further evidence of environmental stabilization at that time. The Zal Sr isotope record exhibits a sustained reduction in Δ(Sr) at the Smithian-Spathian boundary that implies a sustained reduction in weathering rates, consistent with coeval climatic cooling (Fig. 3).

ACKNOWLEDGMENTS

We thank Jonathan Payne and two anonymous reviewers for helpful comments. Sedlacek and Saltzman thank Jeff Linder and Amanda Howard for assistance with $^{87}Sr/^{86}Sr$ analyses. S. Richoz and R. Twitchett provided constructive comments on the manuscript.

Horacek and Brandner thank T. Mohtat and B. Hamdi for organizing the field trip. This is a contribution to International Geoscience Program 572. Algeo gratefully acknowledges support from the Sedimentary Geology and Paleobiology program of the U.S. National Science Foundation, the NASA Exobiology Program, and the China University of Geosciences–Wuhan.

REFERENCES CITED

Albarède, F., Michard, A., Minster, J.F., and Michard, G., 1981, $^{87}Sr/^{86}Sr$ ratios in hydrothermal waters and deposits from the East Pacific Rise at 21°N: Earth and Planetary Science Letters, v. 55, p. 229–236, doi:10.1016/0012-821X(81)90102-3.

Algeo, T.J., and Twitchett, R.J., 2010, Anomalous Early Triassic sediment fluxes due to elevated weathering rates and their biological consequences: Geology, v. 38, p. 1023–1026, doi:10.1130/G31203.1.

Algeo, T.J., Chen, Z.Q., Fraiser, M.L., and Twitchett, R.J., 2011, Terrestrial-marine teleconnections in the collapse and rebuilding of Early Triassic marine ecosystems: Palaeogeography, Palaeoclimatology, Palaeoecology, v. 308, p. 1–11, doi:10.1016/j.palaeo.2011.01.011.

Algeo, T.J., Henderson, C.M., Tong, J., Feng, Q., Yin, H., and Tyson, R.V., 2013, Plankton and productivity during the Permian-Triassic boundary crisis: An analysis of organic carbon fluxes: Global and Planetary Change, v. 105, p. 52–67, doi:10.1016/j.gloplacha.2012.02.008.

Berner, R.A., 2004, The Phanerozoic carbon cycle: CO_2 and O_2: Oxford, UK, Oxford University Press, 150 p.

Brand, U., Posenato, R., Came, R., Affek, H., Angiolini, L., Amzy, K., and Farabegoli, E., 2012, The end-Permian mass extinction: A rapid volcanic CO_2 and CH_4-climatic catastrophe: Chemical Geology, v. 322, p. 121–144, doi:10.1016/j.chemgeo.2012.06.015.

Brayard, A., Escarguel, G., Bucher, H., Monnet, C., Brühwiler, T., Goudemand, N., Galfetti, T., and Guex, J., 2009, Good genes and good luck: Ammonoid diversity and the end-Permian mass extinction: Science, v. 325, p. 1118–1121, doi:10.1126/science.1174638.

Chen, Y., Twitchett, R.J., Jiang, H., Richoz, S., Lai, X., Yan, C., Sun, Y., Liu, X., and Wang, L., 2013, Size variation of conodonts during the Smithian-Spathian (Early Triassic) global warming event: Geology, v. 41, p. 823–826, doi:10.1130/G34171.1.

Erwin, D.H., Bowring, S.A., and Jin, Y.G., 2002, The end-Permian mass extinctions, *in* Koeberl, C., and MacLeod, K.G., eds., Catastrophic events and mass extinctions: Impacts and beyond: Geological Society of America Special Paper 356, p. 363–383, doi:10.1130/0-8137-2356-6.363.

Goddéris, Y., and François, L.M., 1995, The Cenozoic evolution of the strontium and carbon cycles: Relative importance of continental erosion and mantle exchanges: Chemical Geology, v. 126, p. 169–190, doi:10.1016/0009-2541(95)00117-3.

Goddéris, Y., Donnadieu, Y., Le Hir, G., Lefebvre, V., and Nardin, E., 2014, The role of palaeogeography in the Phanerozoic history of atmospheric CO_2 and climate: Earth-Science Reviews, v. 128, p. 122–138, doi:10.1016/j.earscirev.2013.11.004.

Gradstein, F.M., Ogg, J.G., Schmitz, M., and Ogg, G., eds., 2012, The geologic time scale 2012: Boston, Massachusetts, Elsevier, 1176 p.

Hodell, D.A., Mead, G.A., and Mueller, P.A., 1990, Variation in the strontium isotopic composition of seawater (8 Ma to present): Implications for chemical weathering rates and dissolved fluxes to the oceans: Chemical Geology, v. 80, p. 291–307, doi:10.1016/0168-9622(90)90011-Z.

Horacek, M., Richoz, S., Brandner, R., Krystyn, L., and Spötl, C., 2007, Evidence for recurrent changes in Lower Triassic oceanic circulation of the Tethys: The $\delta^{13}C$ record from marine sections in Iran: Palaeogeography, Palaeoclimatology, Palaeoecology, v. 252, p. 355–369, doi:10.1016/j.palaeo.2006.11.052.

Huang, S., Qing, H., Huang, P., Hu, Z., Wang, Q., Zou, M., and Liu, H., 2008, Evolution of strontium isotopic composition of seawater from Late Permian to Early Triassic based on study of marine carbonates, Zhongliang Mountain, Chongqing, China: Science in China Series D: Earth Science, v. 51, p. 528–539, doi:10.1007/s11430-008-0034-3.

Korte, C., Kozur, H.W., Bruckschen, P., and Veizer, J., 2003, Strontium isotope evolution of Late Permian and Triassic seawater: Geochimica et Cosmochimica Acta, v. 67, p. 47–62, doi:10.1016/S0016-7037(02)01035-9.

Korte, C., Kozur, H.W., Joachimski, M.M., Strauss, H., Veizer, J., and Schwark, L., 2004, Carbon, sulfur, oxygen and strontium isotope records, organic geochemistry and biostratigraphy across the Permian/Triassic boundary in Abadeh, Iran: International Journal of Earth Sciences, v. 93, p. 565–581, doi:10.1007/s00531-004-0406-7.

Korte, C., Jasper, T., Kozur, H.W., and Veizer, J., 2006, $^{87}Sr/^{86}Sr$ record of Permian seawater: Palaeogeography, Palaeoclimatology, Palaeoecology, v. 240, p. 89–107, doi:10.1016/j.palaeo.2006.03.047.

Looy, C.V., Brugman, W.A., Dilcher, D.L., and Visscher, H., 1999, The delayed resurgence of equatorial forests after the Permian-Triassic ecological crisis: National Academy of Sciences Proceedings, v. 96, p. 13,857–13,862, doi:10.1073/pnas.96.24.13857.

Martin, E.E., and Macdougall, J.D., 1995, Sr and Nd isotopes at the Permian/Triassic boundary: A record of climate change: Chemical Geology, v. 125, p. 73–99, doi:10.1016/0009-2541(95)00081-V.

Montañez, I.P., Banner, J.L., Osleger, D.A., Borg, L.E., and Bosserman, P.J., 1996, Integrated Sr isotope variations and sea-level history of Middle to Upper Cambrian platform carbonates: Implications for the evolution of Cambrian seawater $^{87}Sr/^{86}Sr$: Geology, v. 24, p. 917–920, doi:10.1130/0091-7613(1996)024<0917:ISIVAS>2.3.CO;2.

Palmer, M.R., and Edmond, J.M., 1989, The strontium isotope budget of the modern ocean: Earth and Planetary Science Letters, v. 92, p. 11–26, doi:10.1016/0012-821X(89)90017-4.

Payne, J.L., and Kump, L.R., 2007, Evidence for recurrent Early Triassic massive volcanism from quantitative interpretation of carbon isotope fluctuations: Earth and Planetary Science Letters, v. 256, p. 264–277, doi:10.1016/j.epsl.2007.01.034.

Payne, J.L., Lehrmann, D.J., Wei, J., Orchard, M.J., Schrag, D.P., and Knoll, A.H., 2004, Large perturbations in the carbon cycle during recovery from the end-Permian extinction: Science, v. 305, p. 506–509, doi:10.1126/science.1097023.

Payne, J.L., Lehrmann, D.J., Wei, J., and Knoll, A., 2006, The pattern and timing of biotic recovery from the end-Permian extinction on the Great Bank of Guizhou, Guizhou Province, China: Palaios, v. 21, p. 63–85, doi:10.2110/palo.2005.p05-12p.

Retallack, G.J., 1995, Permian-Triassic extinction on land: Science, v. 267, p. 77–80, doi:10.1126/science.267.5194.77.

Richter, F.M., and Turekian, K.K., 1993, Simple models for the geochemical response of the ocean to climatic and tectonic forcing: Earth and Planetary Science Letters, v. 119, p. 121–131, doi:10.1016/0012-821X(93)90010-7.

Saito, R., Kaiho, K., Oba, M., Takahashi, S., Chen, Z.Q., and Tong, J., 2013, A terrestrial vegetation turnover in the middle of the Early Triassic: Global and Planetary Change, v. 105, p. 152–159, doi:10.1016/j.gloplacha.2012.07.008.

Song, H.J., et al., 2011, Recovery tempo and pattern of marine ecosystems after the end-Permian mass extinction: Geology, v. 39, p. 739–742, doi:10.1130/G32191.1.

Stanley, S.M., 2009, Evidence from ammonoids and conodonts for multiple Early Triassic mass extinctions: National Academy of Sciences Proceedings, v. 106, p. 15264–15267, doi:10.1073/pnas.0907992106.

Sun, Y.D., Joachimski, M.M., Wignall, P.B., Yan, C.B., Chen, Y.L., Jiang, H.S., Wang, L.N., and Lai, X.L., 2012, Lethally hot temperatures during the Early Triassic greenhouse: Science, v. 338, p. 366–370, doi:10.1126/science.1224126.

Veizer, J., 1989, Strontium isotopes in seawater through time: Annual Review of Earth and Planetary Sciences, v. 17, p. 141–167, doi:10.1146/annurev.ea.17.050189.001041.

Veizer, J., et al., 1999, $^{87}Sr/^{86}Sr$, $\delta^{13}C$ and $\delta^{18}O$ evolution of Phanerozoic seawater: Chemical Geology, v. 161, p. 59–88, doi:10.1016/S0009-2541(99)00081-9.

Waltham, D., and Gröcke, D.R., 2006, Non-uniqueness and interpretation of the seawater $^{87}Sr/^{86}Sr$ curve: Geochimica et Cosmochimica Acta, v. 70, p. 384–394, doi:10.1016/j.gca.2005.09.014.

Ward, P.D., Montgomery, D.R., and Smith, R., 2000, Altered river morphology in South Africa related to the Permian-Triassic extinctions: Science, v. 289, p. 1740–1743, doi:10.1126/science.289.5485.1740.

Wu, H., Zhang, S., Feng, Q., Jiang, G., Li, H., and Yang, T., 2012, Milankovitch and sub-Milankovitch cycles of the early Triassic Daye Formation, south China and their geochronological and paleoclimatic implications: Gondwana Research, v. 22, p. 748–759, doi:10.1016/j.gr.2011.12.003.

Manuscript received 5 February 2014
Revised manuscript received 17 June 2014
Manuscript accepted 28 June 2014

Printed in USA